Recognition of an Unnatural Difluorophenyl Nucleotide by Uracil DNA Glycosylase[†]

Yu Lin Jiang,[‡] Lynda M. McDowell,[§,#] Barbara Poliks,[||] Daniel R. Studelska,[§,#] Chunyang Cao,[‡] Gregory S. Potter,[§] Jacob Schaefer,[§] Fenhong Song,[⊥] and James T. Stivers*[,‡]

Department of Pharmacology and Molecular Sciences, The Johns Hopkins University School of Medicine, 725 North Wolfe Street, Baltimore, Maryland 21205-2185, Department of Chemistry, Washington University, One Brookings Drive, St. Louis, Missouri 63130, Department of Physics, Binghamton University, Binghamton, New York 13902, and The Center for Advanced Research in Biotechnology, University of Maryland Biotechnology Institutes, and The National Institute of Standards and Technology, 9600 Gudelsky Drive, Rockville, Maryland 20850

Received July 28, 2004; Revised Manuscript Received September 27, 2004

ABSTRACT: The DNA repair enzyme uracil DNA glycosylase (UDG) utilizes base flipping to recognize and remove unwanted uracil bases from the genome but does not react with its structural congener, thymine, which differs by a single methyl group. Two factors that determine whether an enzyme flips a base from the duplex are its shape and hydrogen bonding properties. To probe the role of these factors in uracil recognition by UDG, we have synthesized a DNA duplex that contains a single difluorophenyl (F) nucleotide analogue that is an excellent isostere of uracil but possesses no hydrogen bond donor or acceptor groups. By using binding affinity measurements, solution ^{19}F NMR, and solid state ^{31}P{^{19}F} rotational-echo double-resonance (REDOR) NMR measurements, we establish that UDG partially unstacks F from the duplex. However, due to the lack of hydrogen bonding groups that are required to support an open-to-closed conformational transition in UDG, F cannot stably dock in the UDG active site. We propose that F attains a metastable unstacked state that mimics a previously detected intermediate on the uracil-flipping pathway and suggest structural models of the metastable state that are consistent with the REDOR NMR measurements.

Consider that in the three billion base pair human genome, normal DNA bases may be damaged at a startling rate of $\sim 10^3$ events per day per cell (*1*). Due to this relentless and unavoidable spontaneous DNA damage, powerful and exquisitely specific repair glycosylases have evolved to preserve the coding content of the DNA (*2*). How do these enzymes detect rare damaged sites in an enormous background of undamaged DNA? Part of the answer to this formidable specificity problem lies in the remarkable unifying mechanistic feature of all DNA repair glycosylases called damaged base flipping (*3*). Base flipping consists of a coupled conformational change in the enzyme and DNA resulting in a 180° rotation of the entire damaged nucleotide from the DNA duplex into the active site of the enzyme. Damaged base flipping has been observed in the crystal structure of every glycosylase−DNA complex yet studied, which highlights the importance of this transformation in DNA damage recognition (*3*). However, to quantify the specificity of these enzymes it is essential to dissect the multistep process of base flipping and understand the features of damaged bases that promote specific recognition. A premiere system to understand how base flipping leads to specific damage recognition has been the repair enzyme uracil DNA glycosylase (UDG),[1] which locates and excises unwanted uracil bases from DNA without attacking normal DNA bases (*4*).

The pathway for flipping uracil by UDG has been investigated in great detail using both structural and biophysical approaches and has been found to consist of at least three discrete steps (Figure 1) (*5*, *6*). The first step is rapid formation of a weak encounter complex in which the uracil base is still intrahelical ($k_1 = 220\ \mu M^{-1}\ s^{-1}$, $k_{-1} = 600\ s^{-1}$), which is then followed by a metastable state in which the DNA is likely bent but the average position of the uracil base is still largely within the duplex base stack ($k_2 = 700\ s^{-1}$, $k_{-2} = 180\ s^{-1}$). Finally, a conformational docking step ensues in which the enzyme clamps around the fully extrahelical base ($k_3 = 350\ s^{-1}$, $k_{-3} = 100\ s^{-1}$). Thus, formation of the final reactive Michaelis complex requires passage through three specificity gates (Figure 1).

[†] This work was supported by National Institutes of Health Grants GM46835 (J.T.S.) and EB01964 (J.S.).

* To whom correspondence should be addressed. Tel: 410-502-2758. Fax: 410-955-3023. E-mail: jstivers@jhmi.edu.

[‡] The Johns Hopkins University School of Medicine.

[§] Washington University.

[||] Binghamton University.

[#] Current address: Department of Pathology and Immunology, Washington University School of Medicine, 660 S. Euclid Ave., St. Louis, Missouri 63110.

[⊥] The Center for Advanced Research in Biotechnology, University of Maryland Biotechnology Institutes, and The National Institute of Standards and Technology.

[1] Abbreviations: F, 2,4-difluorophenyl nucleotide; Y, pyrene nucleotide; U^{β}, 2′-fluoro-2′-deoxyuridine nucleotide; P, 2-aminopurine nucleotide; DTE, dithioerythritol; COM, center-of-mass; PEG, poly(ethylene glycol); REDOR, rotational-echo double-resonance; UDG, uracil DNA glycosylase.

10.1021/bi0483864 CCC: $27.50
Published on Web 11/12/2004

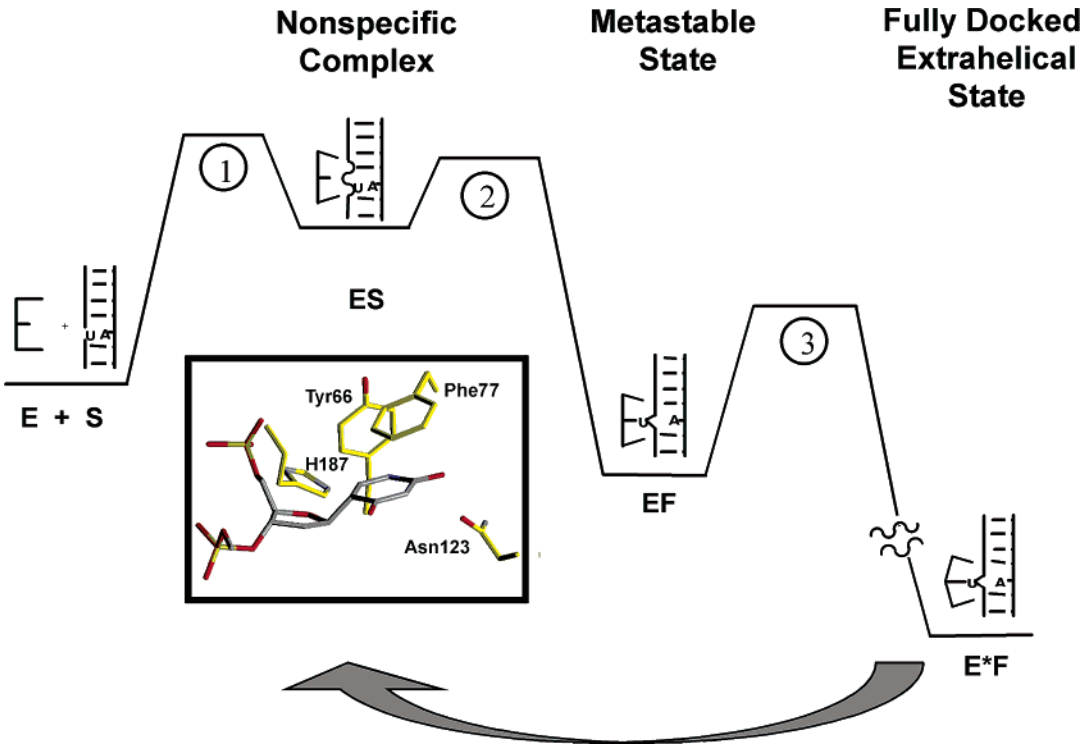

FIGURE 1: Mechanism of uracil flipping by UDG. Stopped-flow fluorescence and other biophysical measurements have revealed a three-step pathway for extruding a uracil base from duplex DNA involving nonspecific DNA binding, a metastable intermediate, and the final fully docked extrahelical state that involves an induced fit conformational change in UDG. The inset shows the active site region of human UDG with a flipped-out pseudo-2′-deoxyuridine analogue (PDB code 1EMH). The active site groups that form specific hydrogen bonds with the uracil base for the *E. coli* enzyme are His187 and Asn123.

It is of interest to understand what structural features of the uracil base lead to specific recognition and flipping. Such structural attributes may promote specificity at early or late steps along the base flipping pathway (Figure 1). At the earliest stages, the weaker hydrogen bonds of U/A or U/G base pairs may increase the equilibrium constant for spontaneous base pair opening (*7*), exposing the base for enzymatic recognition (*8*). At the latest step of uracil flipping, structural studies have suggested that both steric and hydrogen bond complementarities between the enzyme active site and the uracil are important (*9*). Thus, purine bases and thymine are too large to fit in the active site pocket of UDG. However for discrimination between cytosine and uracil, enzymatic recognition of the different hydrogen bond donor and acceptor arrangements of these bases appears to be important (*10*). The role for hydrogen bonding in discriminating between cytosine and uracil is supported by biophysical measurements showing that hydrogen bond complementarity between the base and enzyme active site is essential for catalytic activity (see inset and legend to Figure 1) (*11*).

In this study, we further investigate the role of base hydrogen bonding and sterics in uracil recognition by UDG using a difluorophenyl (F) uracil base analogue that has been incorporated into a DNA context (Figure 2). The F nucleotide has fluorine atoms that closely mimic the van der Waals radii of the O2 and O4 exocyclic oxygen atoms of uracil. However, F lacks the hydrogen bonding groups that would hold it in the DNA duplex as well as in the enzyme active site. Thus, the F nucleotide allows an assessment of the role of hydrogen bonding in the process of base flipping and specificity.

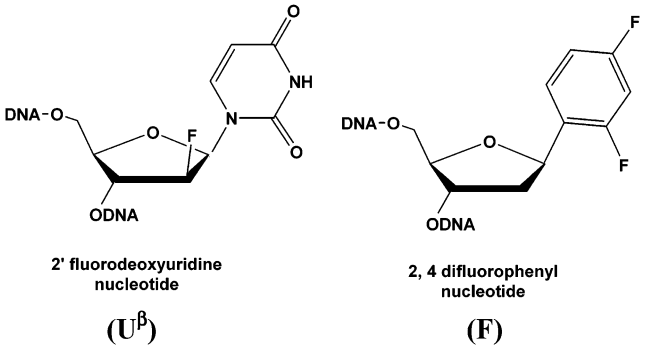

FIGURE 2: Structure of 2′-fluoro-2′-deoxyuridine (U^{β}) and 2,4-difluorophenyl (F) nucleotide analogues. U^{β} is a stable substrate mimic of 2′-deoxyuridine, and F is a close isostere of the uracil base that lacks the hydrogen bonding functional groups.

EXPERIMENTAL PROCEDURES

Enzymes and DNA Substrates. The *Escherichia coli* UDG and the L191A mutant were prepared as previously described (*12*). All of the nucleoside phosphoramidites were obtained from Glen Research (Sterling, VA) except the pyrene nucleoside, which was synthesized as described previously (*13*). In addition, the 2,4-difluorophenyl C-nucleoside phosphoramidite was obtained by a modification of the procedure previously used for preparation of the related difluorotoluenyl C-nucleoside phosphoramidite (*14*). All the reaction conditions were optimized for high yields, and the details of this synthesis have been described (*15*). A key improvement was the use of a new combination catalyst consisting of trifluoroacetic acid−benzenesulfonic acid (5:1 molar ratio) in the epimerization step to avoid decomposition of the reactants. The structure of the final 5′ product was confirmed by proton,

Table 1: Binding of wtUDG and L191A to Duplex DNA Analogues

enzyme	duplex DNA	K_D (μM)	T_m (°C)
wtUDG	PU$^\beta$A/TAT	0.13 ± 0.05[a]	45.8
	PU$^\beta$A/TYT	0.13 ± 0.02	40.0
	PFA/TAT	0.70 ± 0.10	32.9
	PFA/TYT	0.79 ± 0.11	39.9
	PTA/TAT	3.6 ± 0.6	48.2
	PTA/TYT	2.7 ± 0.3	42.8
L191A	PU$^\beta$A/TAT	0.85 ± 0.13	
	PU$^\beta$A/TYT	0.14 ± 0.02	
	PFA/TAT	2.8 ± 0.3	
	PFA/TYT	0.79 ± 0.06	
	PTA/TAT	5.0 ± 0.2	

[a] Previously determined. See ref *12*. Abbreviations: F = difluorophenyl nucleotide; Y = pyrene nucleotide; P = 2-aminopurine nucleotide; U$^\beta$ = 2′-fluoro-2′-deoxynucleotide.

Table 2: Binding of wtUDG to Single-Stranded DNA Sequences[a]

	K_D (μM)
Recognition Strand: 5′-GCGCAZAGTCG-3′	
Z = U$^\beta$	0.21 ± 0.02
Z = F	3.9 ± 0.4
Z = T	19 ± 3
Complementary Strand: 3′-CGCGTXTCAGC-5′	
X = A	23 ± 3
X = Y	18 ± 3

[a] These single-stranded sequences are the two complementary strands of the DNA duplexes shown in Scheme 1 and used in the binding measurements reported in Table 1.

Scheme 1

```
5′-GCGCRZAGTCG-3′
3′-CGCGTXTCAGC-5′
```

fluorine, and ^{31}P NMR and mass spectroscopy: ^{1}H NMR ($CDCl_3$, ppm) δ 7.21−7.54 (m, 12 H); 6.81 (m, 4 H); 5.35 (m, 1 H); 4.52 (m, 1 H); 4.21 (m, 1 H); 3.83 (m, 1 H); 3.79 (s, 6 H); 3.69 (m, 1 H); 3.60 (m, 2 H); 3.29 (m, 2 H); 2.60 (m, 1 H); 2.46 (m, 2 H); 1.95 (m, 1 H); 1.16 (m, 12 H). ^{31}P NMR ($CDCl_3$, ppm) δ 149.36 (s) and 148.90 (s). Mass (ESI) calcd for $C_{41}H_{47}F_2N_2O_6P$ (M + H, M + Na, and M + Cl) 733, 755, and 767; found 733, 755, and 767, respectively.

The 11 base-pair DNA analogues used in the binding, ^{19}F NMR, and REDOR NMR studies were synthesized using standard phosphoramidite chemistry with an Applied Biosystems 390 synthesizer. The oligonucleotides were purified using anion-exchange high-pressure liquid chromatography and were desalted using reversed-phase high-pressure liquid chromatography. The sequences of the duplex DNA molecules are identical except for the central bases in the oligonucleotides (R = A or P, Z = U$^\beta$, T, or F, X = A, Y)[1] (Scheme 1, see also Tables 1 and 2). The DNA strands containing the difluorophenyl nucleotide (F) were characterized by MALDI-TOF-MS (see Table 1): PFA-11, calcd 3345, obsd 3345; AFA-11, calcd 3345, obsd 3344. The characterization of the other strands has been previously reported (*16*). The complementary strands were hybridized in buffer A (10 mM Tris-HCl, 25 mM NaCl, 2.5 mM $MgCl_2$ pH 8.0).

For the imino proton spectra in Figure 3 a second small duplex DNA sequence containing the F nucleotide was used (Scheme 2). This sequence corresponds to the DNA sequence employed by Parikh et al. in their crystallographic studies

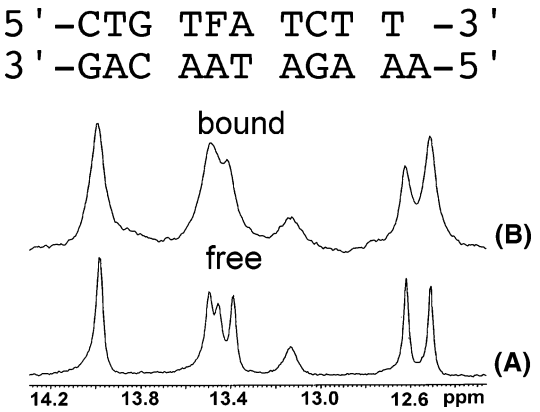

FIGURE 3: 1D imino proton NMR spectra of duplex DNA containing the F nucleotide: (A) imino proton spectra of the free duplex; (B) imino proton spectrum of the DNA complex with UDG. Spectra were collected at 10 °C at a field strength of 500 MHz. The DNA and protein concentrations were 0.25 and 0.3 mM, respectively.

Scheme 2

```
5′-CTGTFATCTT-3′
3′ GACAATAGAAA-5′
```

of the specific UDG−DNA complex except that the deoxypseudouridine was replaced by F and an additional C/G base pair was added for stability (*9*).

DNA Binding Measurements. For determining the binding affinities of the DNA analogues listed in Tables 1 and 2, competitive kinetic inhibition measurements were performed using the substrate ApUpAp (*16*). Conditions were chosen whereby $[UDG]_{tot} \ll [I]$ or [ApUpAp] and [Ap**U**pAp] $\ll K_m$. Accordingly, K_i could be obtained directly from a plot of k/k_o against [I] as shown in eq 1, where k is the observed rate constant ($v/[UDG]_{tot}$) at a given [I] and k_o is the observed rate constant in the absence of the inhibitor (I):

$$k/k_o = 1/(1 + [I]/K_i) \quad (1)$$

For these measurements, a sensitive HPLC kinetic assay for monitoring the formation of the abasic product was employed (*17*). Unless specifically noted, all measurements were performed at 22 °C using buffer A.

Solution ^{19}F NMR Measurements. The one-dimensional ^{19}F NMR experiments on the F-containing DNA oligonucleotides (Tables 1 and 2) were performed at 25 °C on a Varian Gemini 400 spectrometer operating at 376 MHz for fluorine. A 5 mm Varian ^{1}H/^{19}F/^{13}C/^{31}P quadruple resonance probe was used. Spectra were obtained by collecting 22 544 points using 18 867 Hz sweep width, and a recycle delay of 1.5 s between acquisitions. For the free DNA samples and the DNA−enzyme complexes, 3000 and 25 000 scans were collected, respectively. The spectra were processed using exponential multiplication with a line broadening of 30 Hz, followed by Fourier transformation. The samples contained 0.25 mM DNA and 0.3 mM UDG in buffer A. The spectra were referenced to external trifluoroacetic acid.

Fluorescence Measurements. All measurements were performed in buffer A at 25 °C. The maximal increase in 2-aminopurine (P) fluorescence upon enzyme binding was determined by the addition of enzyme to a fixed concentration of DNA containing P (Table 1). Excitation was at 320 nm, and emission spectra from 330 to 450 nm were collected

using a Spex Fluoromax 3 fluorimeter. For tryptophan fluorescence experiments, excitation was at 290 nm, and emission scans were performed over the range 305−450 nm. For the studies using tryptophan fluorescence, the nonfluorescent AU$^{\beta}$A/TAT and AFA/TAT duplexes were used (Table 1).

Modeling of the Extrahelical F Nucleotide. A PFA/TAT B DNA duplex was constructed from the sequence in Scheme 1 using the builder module in Insight II (Accelrys, Inc., San Diego, CA). Since the solution NMR experiments indicated a B DNA conformation for PFA/TAT bound to UDG (see Figure 3), we only considered models that retained this overall conformation. To begin, the crystal structure of human UDG complexed with DNA containing a flipped-out 2′-deoxyuridine analogue (1EMH) (*9*) was used as a guide to create a model of *E. coli* UDG (1EUG) (*18*) bound to PFA/TAT in a canonical B DNA conformation. The 1EUG protein backbone was first superimposed on the protein backbone of 1EMH. Second, the DNA of 1EMH was used as a guide to hand dock PFA/TAT with 1EUG. Next, the 1EUG−PFA/TAT complex was surrounded with a 5 Å layer of water and minimized using the consistent valence force field (cvff). (Comparison of the model protein−DNA complex with additional solid-state NMR results will be published elsewhere.) Finally, the water and protein were eliminated, leaving only the minimized PFA/TAT (model B, Figure 7). Model B has a center-of-mass (COM) dihedral angle for the F nucleotide similar to normal nucleotides in B DNA as reported by Banavali and MacKerell (*19*).

To construct the B DNA models with an extrahelical F nucleotide (models, see Figure 7), F was incrementally rotated from its stacked conformation by adjusting the phosphodiester COM dihedral angles such that the F base rotated out of the base stack through the major groove. During this modeling the DNA conformation was constrained, and only the atoms of the F nucleotide were allowed to move. At each rotation, the F nucleotide was energy-minimized using the molecular mechanics module in DS ViewerPro (Accelrys Inc., San Diego, CA) to eliminate steric conflicts. The base flipping trajectory that resulted from this simple procedure is very similar to that computed by Banavali and MacKerell using potential of mean force calculations (*19*).

Solid State REDOR NMR Sample Preparation. The [*u*-^{15}N] UDG was prepared as previously described (*20*). Dialysis against exchange buffer (100 mM NH_4HCO_3, 1 mM DTE, pH 8.4, at ice temperature) provided [*u*-^{15}N] UDG in a high-salt buffer suitable for both complexation and lyophilization. PFA/TAT (1.39 μmol) and 35.9 mg of [*u*-^{15}N] UDG (1.4 μmol) were incubated for 10 min at ice temperature. Concentrated protectant solution (600 mM trehalose, 6% PEG 8000 in exchange buffer) was added to yield 14 mL of DNA/protein solution in 100 mM NH_4HCO_3, 1 mM DTE, 15 mM trehalose, and 0.2% (w/v) PEG 8000. The use of cryoprotectants (e.g., PEG 8000) and lyoprotectants (e.g., trehalose) in stabilizing proteins during lyophilization has been reviewed (*21*). There is also evidence that trehalose stabilizes DNA during lyophilization (*22*).

The solution, in a 50 mL lyophilization flask, was placed in a −6.5 °C bath and allowed to equilibrate. Initial freezing (slush formation) was observed after the bath temperature was lowered to −7 °C. The temperature was then gradually lowered to −30 °C. The flask was attached to vacuum, and lyophilization was conducted at lowered temperatures for 4 days and at RT for 2 days. Details of the custom lyophilization apparatus have been published (*23*).

The volatile NH_4HCO_3 was removed during lyophilization. The estimated anhydrous weight of protein, DNA, and nonvolatile buffer components was 153.5 mg. Tightly bound water, typically ∼10 wt %, is retained in lyophilized samples. This implies that 15 mg of water should be added to the anhydrous weight above to obtain the total sample weight. The distribution of retained water molecules among protein, DNA, and other buffer components is not known.

The sample was packed into a 5-mm outside-diameter, thin-wall, zirconium pencil rotor (Varian) under dry nitrogen gas. Assuming a typical sample handling loss of 10%, the weight of the packed sample (148.7 mg) is consistent with a hydration level of ∼10 wt %. Care was taken to avoid absorption of atmospheric water, which can lead to reduced ^{31}P chemical shift tensors arising from large amplitude molecular motion (*24*) (see Results). The sample was stored at −80 °C when not in the spectrometer.

REDOR Spectroscopy. Rotational-echo double-resonance (REDOR) restores heteronuclear dipolar couplings in the presence of magic-angle spinning (MAS) (*25*, *26*). Numerous reviews of the biological applications of REDOR and other solid-state NMR methods are available (*27*−*30*). Studies of DNA using REDOR have also been reported (*31*, *32*). When lyophilized dodecamer samples contained 3−14 waters per nucleotide, it was reported that the intensity of the distribution of ^{31}P spinning sidebands did not change and that the REDOR measurements yielded results comparable to crystallography (*31*). To our knowledge, this is the first application of REDOR to a protein/DNA complex.

REDOR spectra are collected pairwise by alternate scans. One spectrum (S) has rotor-synchronized dephasing pulses and the other (S_0 or full echo) does not. The dephasing pulses interfere with the MAS spatial averaging by changing the sign of the heteronuclear dipolar coupling. Thus, S is smaller than S_0. All the observed nuclei contribute to the S_0, or full echo, spectrum. The shorthand observed {dephasing nucleus} is used to specify the nuclei in REDOR experiments. The REDOR difference spectrum ($\Delta S = S_0 - S$) is dominated by the observed nuclei with the strongest dipolar couplings (and shortest distances) to the dephasing nuclei. But nuclei farther away will also contribute. For example, a single ^{31}P that is 16 Å from a single ^{19}F has a $\Delta S/S_0 \approx 0.01$ when the ^{31}P{^{19}F} REDOR evolution time is 8 ms (*33*).

For the most accurate distances, the REDOR experiment is performed at multiple evolution times. The ratio $\Delta S/S_0$ normalizes data collected at different evolution times for relaxation effects and instrument drift. For ^{31}P{^{19}F} REDOR, the integrated intensity over all the spinning sidebands and the center band was used to compute the ratio. The $\Delta S/S_0$ data were compared with the calculated REDOR dephasing (*34*) for 1EMH (*9*) and the structural models described above. To calculate the 1EMH REDOR dephasing, the O2 and O4 atoms of the extrahelical uracil were assumed to occupy the same positions that the ^{19}F of the difluorophenyl base would occupy.

Spectrometer. REDOR NMR was performed using a six-frequency transmission-line probe (*35*) having a 12-mm long, 6-mm inside-diameter analytical coil and a Chemagnetics/

Varian ceramic stator. MAS was either 7143 or 4167 Hz. For all experiments, MAS was under active control to within ±2 Hz. A stack-mounted air chiller cooled the rotor to an exit-gas temperature of −5 ± 1 °C. The spectrometer was controlled by a Tecmag pulse programmer. Radio frequency pulses for ^{31}P (202 MHz) were produced by a 1-kW American Microwave Technology power amplifier. Proton (500 MHz) and ^{19}F (470 MHz) radio frequency pulses were generated by 1-kW Amplifier Systems tube amplifiers driven by 50-W American Microwave Technology power amplifiers. A 12-T static magnetic field was provided by an 89-mm bore Magnex superconducting solenoid.

The π-pulse lengths were 6.0 μs for ^{31}P and 5.0 μs for ^{19}F. Proton−^{31}P cross-polarization transfers were made in 1.2 ms with radio frequency fields of 83.3 kHz. The ^{31}P spectra were acquired with a dwell time of 8.75 μs. The digital spectral width corresponded to the dwell time, but an external filter was used to obtain an effective spectral width of ±40 kHz. ^{31}P{^{19}F} REDOR spectra were collected with continuous wave decoupling and standard xy-8 phase cycling on both the ^{31}P and ^{19}F channels (*36*, *37*). The recycle delay was 3 or 4 s.

RESULTS

Characterization of Duplexes Containing the F Nucleotide. The 11-mer duplex scaffold that is employed in these studies has been used in extensive studies of the base flipping mechanism of wtUDG and several mutants (*5*, *6*). Because of the short length of these duplexes and the introduction of destabilizing unnatural F/A and F/Y base pairs (where Y is pyrene nucleotide), we assessed the duplex stabilities in melting experiments before determining their binding affinities to UDG. The T_m values fell in the range 32.9−45.8 °C (Table 1) with the PFA/TAT duplex having the lowest stability (see Table 1 for duplex DNA abbreviations). Accordingly, to ensure binding to the duplex forms, the competitive binding measurements were performed at 22 °C, which is 11 °C below the melting temperature of the least stable duplex.

We investigated the imino proton NMR spectra of another similar 10-mer duplex that contained the F nucleotide to determine whether binding of UDG dramatically altered the conformation of the duplex. In the absence of UDG, this duplex shows nine of the expected 10 imino resonances (Figure 3A). Upon the addition of 1 equiv of UDG (Figure 3B), significant imino proton line broadening occurs, as expected for the formation of a large protein−DNA complex, but the imino chemical shifts are unperturbed from their values in the free DNA. This result indicates that no large perturbation of the B DNA structure occurs upon UDG binding to DNA that contains an F nucleotide.

Relative Binding Affinity of the Difluorophenyl Nucleotide. We have previously found that 2′-fluoro-2′-deoxyuridine (U$^{\beta}$) is an excellent substrate mimic for UDG that is resistant to glycosidic bond cleavage due to the extreme destabilization of the positive charge that develops on the anomeric carbon during the reaction by the electronegative 2′-fluorine atom (*38*). The availability of this stable substrate analogue has provided a key tool for study of the base flipping mechanism of UDG (*5*, *6*). To evaluate the relative binding affinity of F to UDG, we measured the binding affinities of three DNA analogues that contained either the specific recognition base (U$^{\beta}$), the nonpolar uracil isostere (F), or the normal base T, all in the context of a base pair with adenine (Table 1). A convenient method to determine the binding affinity of these analogues is our previously described competitive kinetic inhibition assay (*12*, *16*). As shown in Figure 4 (open circles), DNA containing the specific U$^{\beta}$/A recognition site competitively inhibits cleavage of substrate DNA with a $K_D = 0.13$ μM (Table 1). We also found that the same DNA containing the F/A site competitively inhibited the reaction with an affinity only 5-fold less than the specific sequence (Figure 4, closed circles). In contrast, nonspecific DNA containing a T/A base pair bound 28-fold more weakly than the construct with the U$^{\beta}$/A site ($K_D = 3.6$ μM), suggesting that properties of the F/A site lead to enhanced binding even in the absence of hydrogen bonding groups. The relative binding affinities are reproduced when these base analogues are presented in a single-stranded DNA context, although the absolute affinities are weaker than the duplex constructs (Table 2). The weaker affinity likely reflects the higher conformational entropy of the free single DNA strands as compared to the duplex molecules.

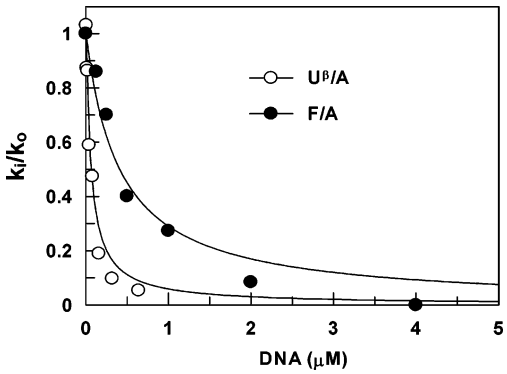

FIGURE 4: Binding affinity of UDG for DNA containing a F/A and U$^{\beta}$/A base pair. Competitive kinetic inhibition experiments were employed to determine the binding affinities of the DNA analogues listed in Tables 1 and 2. The lines are nonlinear regression best-fits to eq 1.

The F Nucleotide Attains a Metastable Unstacked State: Fluorescence Studies. Since UDG has been shown to place U$^{\beta}$ in at least two detectable conformational states—a metastable state and the final extrahelical state—we wanted to ascertain the nature of the state that was attained by the unnatural F nucleotide (Figure 1). Previous work has established that the metastable state can be detected by an increase in 2-aminopurine (P) fluorescence of the DNA upon UDG binding (Figure 5A, solid line spectra), and the final docked state is characterized by a tryptophan fluorescence quenching of UDG (Figure 5B, solid line spectra) (*6*). The free PFA/TAT duplex has a 2-aminopurine fluorescence intensity about 10-fold greater than PU$^{\beta}$A/TAT, which indicates that on average the 2-aminopurine probe in PFA/TAT is less stacked with the neighboring DNA bases than in PU$^{\beta}$A/TAT. Addition of 1 equiv of UDG to PFA/TAT results in only a small increase in P fluorescence (Figure 5A, dashed line spectra), presumably because the fluorescence was already high in the free DNA. The UDG tryptophan fluorescence does not change upon binding of AFA/TAT (Figure 5B, dashed line spectrum), which differs significantly from the 1.8-fold decrease in fluorescence when AU$^{\beta}$A/TAT binds to UDG (Figure 5B). These data suggest

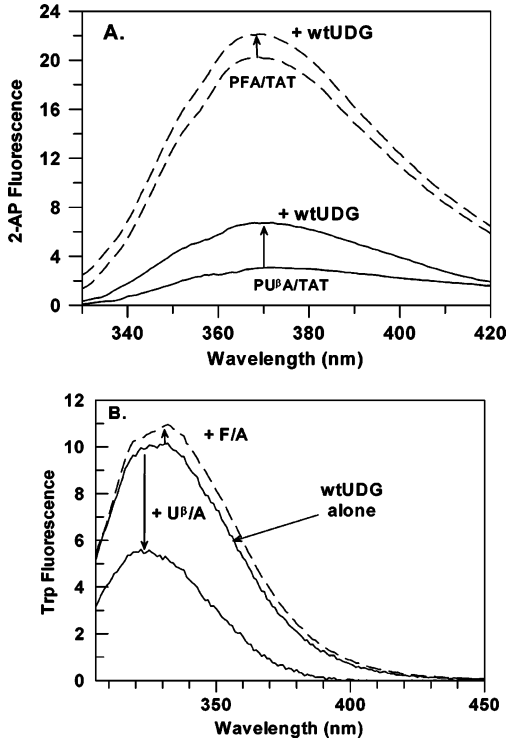

FIGURE 5: 2-Aminopurine and tryptophan fluorescence studies of F/A and U^{β}/A binding to UDG: (A) 2-aminopurine (P) fluorescence changes of the PFA/TAT (dashed lines) and $PU^{\beta}A$/TAT (solid lines) DNA constructs upon binding to wtUDG; (B) tryptophan fluorescence changes of wtUDG upon binding to DNA that contains a U^{β}/A base pair (solid line) or a F/A base pair (dashed line).

that F may attain the metastable state but cannot induce the final conformational change in UDG (step 3, Figure 1).

Binding of F Requires the Leu191 Base Flipping Wedge of UDG. A hallmark of the base flipping mechanism of UDG is the pushing role of the conserved residue, Leu191, which projects into the minor groove and expels the uracil base through the major groove (*39*). Accordingly, substitution of Leu191 with alanine decreases the binding affinity of UDG to DNA that contains a specific U^{β}/A recognition site (*12*) and also prevents UDG from attaining the closed conformation in which the base is fully docked in the active site pocket (step 3, Figure 1). The L191A mutation can be fully rescued when a bulky pyrene nucleotide wedge group (Y) is placed opposite to U^{β} in the substrate (i.e., a U^{β}/Y base pair). The rescue effect is an example of substrate preorganization, where the concentration of the reactive extrahelical conformation is increased by its extrusion from the DNA base stack by pyrene.

To further substantiate that F utilizes the same base flipping pathway as uracil, we evaluated whether its binding affinity was diminished by the removal of Leu191 and whether the mutational effect could be rescued using a substrate with a F/Y base pair as observed previously with the U^{β} substrate analogue (*12*). As shown in Table 1, the L191A mutation reduces the binding affinity of the F/A and U^{β}/A analogues by nearly identical amounts (4−6.5-fold), and the damaging effect of the mutation is rescued when F or U^{β} are presented in the context of a pyrene base pair. In contrast, the binding affinity of wild-type UDG is not affected by whether U^{β}, F, or T is presented in the context of a pyrene or adenine base pair because the native Leu191 pushing group is intact (Table 1). The rescue effect is not due to a special affinity of UDG for the pyrene strand because this single strand binds with weak affinity, just like the analogous adenine containing strand (Table 2). These findings strongly suggest that the mechanism of F recognition involves the Leu191 side chain, in a similar manner as U^{β}.

The F Nucleotide Attains a Metastable Unstacked State: ^{19}F Solution NMR Studies. The above binding, mutagenesis, and chemical rescue experiments indicate that UDG can specifically recognize F using a mechanism involving the Leu191 wedge, but these studies provide little information about whether F attains an extrahelical state. To address this question, we turned to ^{19}F NMR measurements. Comparison of the ^{19}F NMR spectrum of F in single-stranded (ssF) and in duplex forms (PFA/TAT and PFA/TYT) provides diagnostic chemical shifts for the 2- and 4-fluorine atoms in a stacked and unstacked state (Figure 6). The 2- and 4-fluorine atoms resonate at −39.2 and −35.2 ppm in ssF (Figure 6a) but are shifted upfield by 1.5 and 0.5 ppm in the F/A duplex, reflecting the magnetic shielding effect from base π electron clouds in the DNA duplex (Figure 6b). When F is placed opposite to the pyrene nucleotide in the F/Y duplex (Figure 6c), the downfield ^{19}F shifts previously observed in ssF return, presumably because pyrene displaces F into unstacked conformation with similar chemical shifts as ssF. When 1 equiv of UDG binds, the 2-fluorine in PFA/TAT is shifted downfield to a new chemical shift that falls between that of the free PFA/TAT duplex and ssF (Figure 6d), suggesting that the average conformation of F is partially unstacked when UDG is bound. Finally, when 1 equiv of UDG binds to PFA/TYT, the 2-fluorine assumes a chemical shift identical to that of free ssF (Figure 6e), suggesting that pyrene shifts the equilibrium to favor the extrahelical state. In addition, the 4-fluorine of the PFA/TYT duplex shows slow exchange between at least two chemical shift environments when bound to UDG, indicating that a dynamic process is being observed (see Discussion).

If UDG uses the same mechanism to unstack the F nucleotide and uracil, then it would be expected that (i) the ^{19}F shifts of PFA/TAT in complex with the L191A mutant would be unchanged from that of free PFA/TAT due to the damaging effect of L191A on base flipping and that (ii) the L191A complex with PFA/TYT would have ^{19}F shifts indicative of an unstacked state due to pyrene rescue (see above). In complete accord with these expectations, the ^{19}F shifts of the PFA/TAT-L191A complex are identical to the free F/A duplex (Figure 6f), and the ^{19}F shifts of the PFA/TYT−L191A complex are similar to wtUDG, including the slow exchange dynamics of the 4-fluorine resonance (Figure 6g).

Dynamics of the Bound F Nucleotide. The solution ^{19}F NMR data provide evidence for rapid dynamics of the bound F nucleotide. The ^{19}F chemical shift of the bound AFA/TAT duplex is intermediate to that of free AFA/TAT and single-stranded ssF DNA (Figures 6d and 5a,b), indicating rapid chemical shift averaging between a stacked and unstacked state. The chemical shift difference between ssF and AFA/TAT ($\Delta\nu = 540$ Hz) may be used to calculate a lower limit on the exchange rate between these two states using eq 2 (*40*), from which a value of $k_{ex} > 1200$ s^{-1} is obtained. This

$$k_{ex} > 0.7\pi\Delta\nu \qquad (2)$$

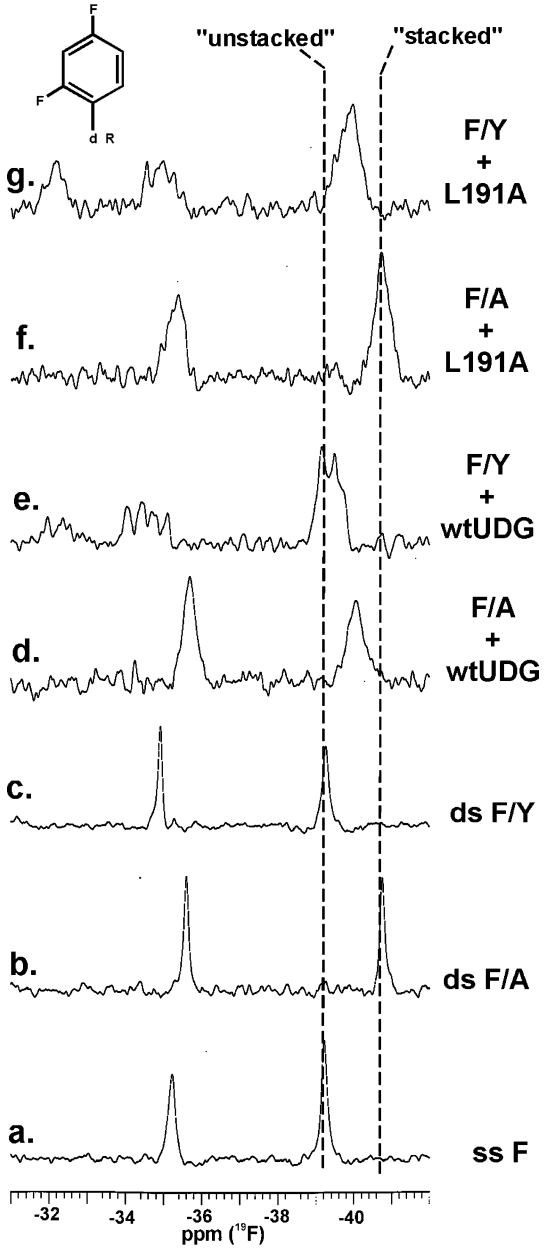

FIGURE 6: ^{19}F NMR studies of difluorophenyl (F) nucleotide binding to UDG: (a) single-stranded DNA containing F (ssF); (b) free PFA/TAT duplex DNA; (c) free PFA/TYT duplex DNA; (d) PFA/TAT duplex bound to wtUDG; (e) PFA/TYT duplex bound to wtUDG; (f) PFA/TAT duplex bound to L191A UDG; (g) PFA/TYT duplex bound to L191A UDG. All of the complexes in this figure were formed using about 200 μM concentrations of DNA and enzyme. These concentrations are several orders of magnitude greater than the K_D values of the enzyme for the DNA. Thus, the DNA constructs are 100% in the bound state.

lower limit for the exchange rate is faster than rates of spontaneous base pair opening in B DNA, which typically fall in the range 200−1000 s^{-1} for T/A base pairs and 20−100 s^{-1} for G/C base pairs (*41*). Despite its rapid exchange between a stacked and unstacked state and the absence of stabilizing hydrogen bonds, F still spends a significant time within the DNA base stack.

Structural Characterization of the Unstacked F Nucleotide Using $^{31}P\{^{19}F\}$ REDOR NMR. We used REDOR NMR to obtain structural information of the PFA/TAT duplex bound to *E. coli* UDG. (Our attempts to grow crystals of this complex were unsuccessful.) We believe that the solid-state measurements reflect the solution behavior of this complex based on the following four pieces of evidence (see also Experimental Procedures). First, the sample preparation and stabilization procedures were optimized to preserve protein and DNA structure (see Experimental Procedures). Second, since molecular motion arising from excessive hydration of the DNA phosphodiester groups would cause the REDOR measurements to overestimate the distance between nuclei, we measured the ^{31}P chemical shift tensor of the DNA, which remained full and constant over the course of the experiments (not shown). This result indicates that no large amplitude molecular motions of the phosphodiester backbone were occurring that might bias the distance measurements (*31*). Third, the enzyme was found to retain most of its activity even after 2 years in the sample rotor. Not accounting for handling losses, which typically are around 10−15%, the rehydrated NMR sample retained 60% of the original enzymatic activity in a standard activity assay (not shown). Finally, the structures that were calculated from the REDOR measurements were entirely consistent with the solution NMR results and other structural and computational studies on base flipping (*7*, *8*, *19*).

The $^{31}P\{^{19}F\}$ REDOR dephasing data ($\Delta S/S_0$) for the PFA/TAT−UDG complex are shown as solid circles in Figure 7A,B, along with the calculated REDOR dephasing curves for six structural models. Since the 1D imino proton spectra indicate that the duplex containing the F nucleotide remains in the B DNA conformation when bound to UDG (Figure 3), we only considered structural models for PFA/TAT with an overall B DNA conformation (models B, 1, 2, 3, and 4 in Figure 7A,B). The model corresponding to the structure of the uracil-containing DNA bound to UDG (1EMH) was obtained by substituting the uracil in 1EMH with the F nucleotide analogue (see Experimental Procedures). Using this approach, we could determine which of these models were most consistent with the REDOR dephasing data.

We first considered models in which the F nucleotide is in a single conformation while bound to UDG (Figure 7A,B, models B, 1−4, and 1EMH). When this analysiswas used, the models in Figure 7A corresponding to B DNA (red dots), model 2 (pink line), and model 3 (light green line) most closely matched the data, while models 1, 4, and 1EMH deviate significantly. Although a single stacked state of the F nucleotide is also consistent with the REDOR dephasing data, such a conformation (model B, Figure 7A,B) is not consistent with the solution NMR results that indicate unstacking of the F nucleotide (see above). Thus, models 2 and 3 represent possible unstacked conformations of F when bound to UDG.

Because solution NMR measurements indicate fast dynamic averaging of intrahelical and extrahelical conformations of the F nucleotide (Figure 6), the process of freezing and lyophilization would be expected to trap a mixture of stacked and unstacked F nucleotide conformations in the lyophilized solid. The REDOR dephasing for a mixture of conformations is the appropriately weighted sum of each conformation's dephasing. Thus, an equally populated mixture of models 2 and B would have a calculated REDOR dephasing curve that falls midway between the red dots and the solid pink line in Figure 7A and would clearly account for the observed data. Likewise, a sample mixture containing an equal population of models 3 and B yields a REDOR

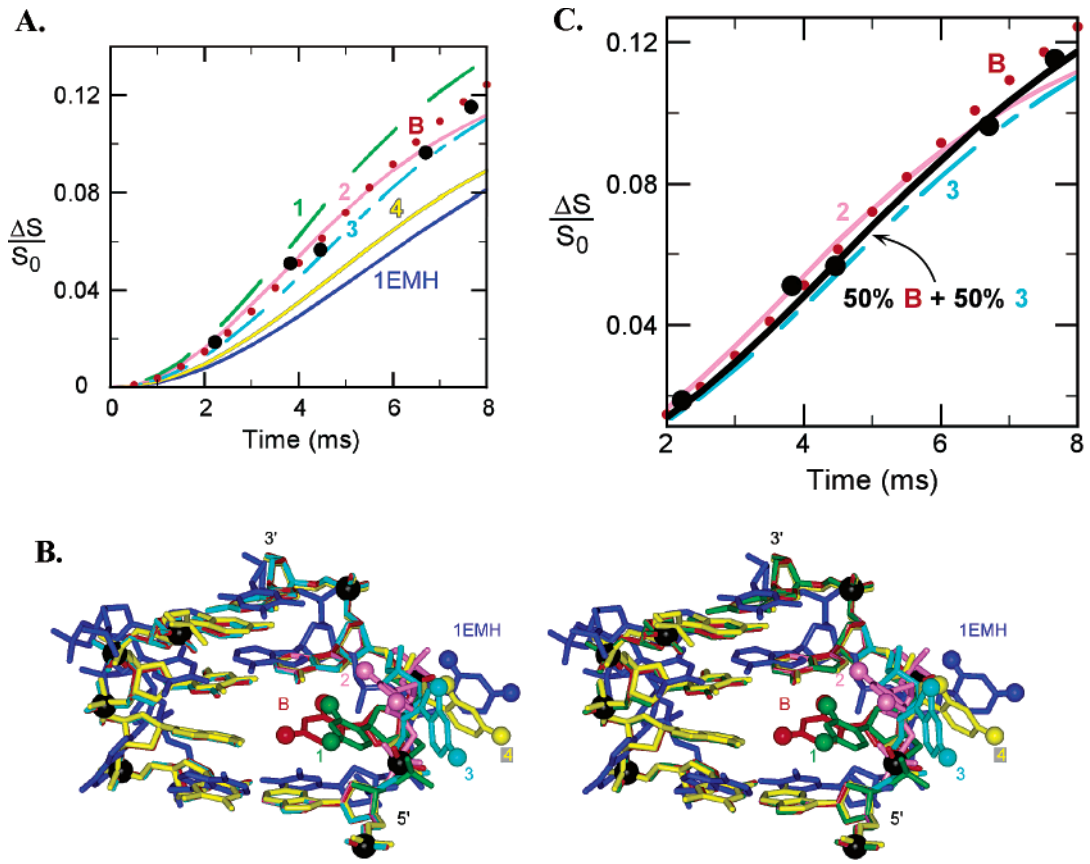

Model structure	B	1	2	3	4
COM dihedral (see Fig. 1B in Ref 19)	33	66	115	159	175

FIGURE 7: REDOR spectroscopy of the UDG complex with AFA/TAT and structure models of the stacked and unstacked F nucleotide. Panel A shows 121 MHz $^{31}P\{^{19}F\}$ REDOR dephasing ($\Delta S/S_0$) for all DNA phosphates contributing to the observed signal of PFA/TAT complexed with UDG. The six curves correspond to the expected dephasing calculated using the structural models of panel B. Panel B shows structural models of the fully stacked (red) and four partially unstacked (green, pink, aqua, and yellow) difluorophenyl nucleotide conformations**.** The conformation of the flipped uracil in the crystal structure 1EMH is also shown in dark blue. The labels and colors match those of the calculated dephasing curves shown in panel A. Tables of selected $^{31}P-^{19}F$ distances and coordinates are available as Supporting Information. The center of mass dihedral angle for each flipped nucleotide as defined by Banavali and MacKerrell (*19*) is shown in the table below the family of structural models. Panel C shows a zoomed view of selected REDOR curves from panel A and the calculated REDOR dephasing curve for a 1:1 mixture of model B and model 3 (black line).

dephasing curve as shown in Figure 7C (black line), which fits the dephasing data nearly perfectly. Because the average solution ^{19}F chemical shift (Figure 6d) indicates that the stacked and unstacked populations are nearly equal in solution, the dynamically interchanging conformations are most likely represented by an equal mixture of model B with extrahelical conformations resembling models 2 or 3.

DISCUSSION

Hydrogen Bond Compensation during Uracil Flipping. One approach to uncover how binding energy is used during uracil flipping is to remove interactions that are important in the initial and final states (i.e., the free DNA and the final extrahelical state) and ask how the deletion affects the overall binding equilibrium. With respect to the F nucleotide, all hydrogen bonding interactions are ablated, but aromatic stacking interactions are relatively unperturbed as compared to the native uracil base. Thus, if the hydrogen bonds of uracil are energetically equivalent in the DNA duplex and in the enzyme active site, then the free energy cost of breaking the hydrogen bonds in DNA during base flipping would be fully paid for by their restoration when the base enters the active site. The similar binding affinities of the U^{β} and F nucleotides suggest that such an energy tradeoff is occurring during base flipping. This result leads to the conclusion that normal bases are protected from adventitious flipping by the strength of their hydrogen bonding interactions in the duplex (*8*).

The Nature of the Unstacked Conformation of the F Nucleotide. The solution NMR, REDOR NMR, and fluorescence spectroscopy studies provide a consistent picture of the extrahelical state that is attained by the F nucleotide. The ^{19}F chemical shift of the 4-fluorine atom of bound AFA/TAT assumes an intermediate value between that of ssF and the free AFA/TAT duplex (Figure 6), indicating that the average conformation of the enzyme-bound F nucleotide is partially unstacked. Consistent with the solution NMR results, the REDOR NMR dephasing curves are best modeled using two conformations of the difluorophenyl nucleotide reflecting a stacked and partially unstacked state (Figure 7). Finally, the 2-aminopurine and tryptophan fluorescence data indicate that the F nucleotide is unstacked but that it is not

stably docked in the active site pocket (Figure 5). The absence of a tryptophan fluorescence decrease in UDG indicates that the F nucleotide is unable to evoke the clamping motion of UDG that occurs for DNA that contains the U^{β} nucleotide (Figure 5B). This result is fully compatible with previous mutagenesis studies of UDG where it was discovered that hydrogen bonds between an active site asparagine residue (Asn123, Figure 1) and uracil O4 and H3 were essential to educe the closed conformation of the enzyme (*5*). Moreover, the observation that the F nucleotide requires the bulky side chain of Leu191 to attain a partially extrahelical state (Figure 6f) yet cannot attain the fully extrahelical conformation as does uracil provides further evidence that Leu191 plays a "pushing" role in the formation of an early metastable unstacked state in the process of uracil flipping (*5*). Taken together, these findings indicate that the F nucleotide assumes an average conformation that is intermediate between B DNA and the fully extrahelical state observed in the crystal structure of UDG and uracil-containing DNA (compare red and blue structures in Figure 7B). The average conformation of the F nucleotide may resemble that of the structurally uncharacterized metastable state of uracil that has been detected in rapid kinetic studies of UDG (Figure 1) (*5*, *6*).

We conclude that the favorable steric features of the F base and its lack of stabilizing hydrogen bonds are sufficient to allow formation of the metastable intermediate. However, specific hydrogen bonding interactions are required to form the catalytically productive Michaelis complex. Given this multistep recognition mechanism that selects on the basis of steric and hydrogen bonding features of the base, it is unlikely that other normal DNA bases can form catalytically productive extrahelical states when bound to UDG.

The Basis of UDG Catalytic Specificity. The multistep uracil recognition strategy that is used by UDG ultimately provides at least a 10^6-fold discrimination against cleavage of the glycosidic bond of any other nucleoside (*8*). In contrast with site-specific DNA binding proteins, less than 10^2-fold of the specificity of UDG is found at the binding step (Tables 1 and 2). Comparison of the binding affinities of the specific and nonspecific DNA constructs shows that the specific U^{β} analogue binds 27-fold to 100-fold more tightly than the nonspecific DNA containing T. This result indicates that base flipping does not result in interactions that lead to extraordinarily tight ground state binding as compared to nonspecific DNA and that a large fraction of the available binding energy is used to overcome thermodynamically unfavorable events during the base flipping process (see Discussion above). Such events include breaking of the Watson−Crick hydrogen bonds in the DNA duplex as the base is extruded, destabilization of the DNA base stacking interactions, and unfavorable distortions in the DNA structure that are required for base flipping (*8*).

The above observations indicate that the remaining $>10^4$-fold catalytic discrimination between specific and nonspecific substrates must be achieved by selective stabilization of 2′-deoxyuridine in the transition state. Since UDG follows a dissociative mechanism in which the uracil base assumes a full negative charge and the 2′-deoxyribose a full +1 charge in the transition state, specific interactions that stabilize these electronic features would lead to enhanced specificity. It has been previously established that phosphodiester electrostatic interactions are important for stabilization of the positively charged sugar (*17*, *42*, *43*) and that a neutral catalytic histidine is key for stabilizing the negative charge that develops on the base (*20*, *44*−*46*). However, in terms of *selective* transition-state stabilization for cleavage of 2′-deoxyuridine relative to other nucleotides, the phosphodiester electrostatic interactions would not be expected to be as important as the highly specific hydrogen bonds to the uracil base. Thus, the conformational clamping step comprises the final gateway to the uracil-specific hydrogen bonding network of UDG (step 3, Figure 1). The subsequent step of glycosidic bond cleavage involves strengthening of these hydrogen bonds as the C−N bond is cleaved, and the negative charge migrates onto the base heteroatoms in the transition-state. The specific transition-state stabilization provided by these catalytic interactions is likely the largest energetic contribution to the specificity of UDG.

ACKNOWLEDGMENT

We thank members of the Stivers laboratory for reading the manuscript, and Chris Gross for assistance with the fluorine NMR measurements.

SUPPORTING INFORMATION AVAILABLE

Tables containing the identities of the phosphorus atoms closest to the fluorines of each model and their corresponding P−F distances and coordinates and selected longer range P−F distances and coordinates. This information is available free of charge via the Internet at http://pubs.acs.org.

REFERENCES

1. Lindahl, T., and Nyberg, B. (1974) Heat-induced deamination of cytosine residues in deoxyribonucleic acid, *Biochemistry 13*, 3405−3410.
2. Stivers, J. T., and Jiang, Y. L. (2003) A mechanistic perspective on the chemistry of DNA repair glycosylases, *Chem. Rev. 103*, 2729−2759.
3. Stivers, J. T. (2004) Site-specific DNA damage recognition by enzyme-induced base flipping, *Prog. Nucleic Acid Res. Mol. Biol. 77*, 37−65.
4. Stivers, J. T., and Drohat, A. C. (2001) Uracil DNA glycosylase: insights from a master catalyst, *Arch. Biochem. Biophys. 396*, 1−9.
5. Jiang, Y. L., Song, F., and Stivers, J. T. (2002) Base flipping mutations of uracil DNA glycosylase: substrate rescue using a pyrene nucleotide wedge, *Biochemistry 41*, 11248−11254.
6. Jiang, Y. L., and Stivers, J. T. (2002) Mutational analysis of the base flipping mechanism of uracil DNA glycosylase, *Biochemistry 41*, 11236−11247.
7. Gueron, M., Kochoyan, M., and Leroy, J. L. (1987) A single mode of DNA base-pair opening drives imino proton exchange, *Nature 328*, 89−92.
8. Krosky, D. J., Schwarz, F. P., and Stivers, J. T. (2004) Linear free energy correlations for enzymatic base flipping: how do damaged base pairs facilitate specific recognition? *Biochemistry 43*, 4188−4195.
9. Parikh, S. S., Walcher, G., Jones, G. D., Slupphaug, G., Krokan, H. E., Blackburn, G. M., and Tainer, J. A. (2000) Uracil-DNA glycosylase-DNA substrate and product structures: conformational strain promotes catalytic efficiency by coupled stereoelectronic effects, *Proc. Natl. Acad. Sci. U.S.A. 97*, 5083−5088.
10. Kavli, B., Slupphaug, G., Mol, C. D., Arvai, A. S., Peterson, S. B., Tainer, J. A., and Krokan, H. E. (1996) Excision of cytosine and thymine from DNA by mutants of human uracil-DNA glycosylase, *EMBO J. 15*, 3442−3447.
11. Kwon, K., Jiang, Y., and Stivers, J. (2003) Rational engineering of a DNA glycosylase specific for an unnatural cytosine:pyrene base pair, *Chem. Biol. 10*, 1−20.

12. Jiang, Y. L., Kwon, K., and Stivers, J. T. (2001) Turning on uracil-DNA glycosylase using a pyrene nucleotide switch, *J. Biol. Chem. 276*, 42347−42354.
13. Jiang, Y. L., and Stivers, J. T. (2003) Efficient epimerization of pyrene and other aromatic C-nucleosides with trifluroacetic acid in dichloromethane, *Tetrahedron Lett. 44*, 85−88.
14. Moran, S., Ren, R. X. F., Rumney, S., and Kool, E. T. (1997) Difluorotoluene, a nonpolar isostere for thymine, codes specifically and efficiently for adenine in DNA replication, *J. Am. Chem. Soc. 119*, 2056−2057.
15. Jiang, Y. L., and Stivers, J. T. (2003) Novel epimerization of aromatic C-nucleosides with electron-withdrawing substituents with trifluoroacetic acid-benzene-sulfonic acid using mild conditions, *Tetrahedron Lett. 44*, 4051−4055.
16. Jiang, Y. L., Drohat, A. C., Ichikawa, Y., and Stivers, J. T. (2002) Probing the limits of electrostatic catalysis by uracil DNA glycosylase using transition-state mimicry and mutagenesis, *J. Biol. Chem. 277*, 15385−15392.
17. Jiang, Y. L., and Stivers, J. T. (2001) Reconstructing the substrate for uracil DNA glycosylase: tracking the transmission of binding energy in catalysis, *Biochemistry 40*, 7710−7719.
18. Xiao, G., Tordova, M., Jagadeesh, J., Drohat, A. C., Stivers, J. T., and Gilliland, G. L. (1999) Crystal structure of *Escherichia coli* uracil DNA glycosylase and its complexes with uracil and glycerol: structure and glycosylase mechanism revisited, *Proteins: Struct., Funct., Genet. 35*, 13−24.
19. Banavali, N. K., and MacKerell, A. D., Jr. (2002) Free energy and structural pathways of base flipping in a DNA GCGC containing sequence, *J. Mol. Biol. 319*, 141−160.
20. Drohat, A. C., Xiao, G., Tordova, M., Jagadeesh, J., Pankiewicz, K. W., Watanabe, K. A., Gilliland, G. L., and Stivers, J. T. (1999) Heteronuclear NMR and crystallographic studies of wild-type and H187Q *Escherichia coli* uracil DNA glycosylase: electrophilic catalysis of uracil expulsion by a neutral histidine 187, *Biochemistry 38*, 11876−11886.
21. Arakawa, T., Prestrelski, S. J., Kenney, W. C., and Carpenter, J. F. (2001) Factors affecting short-term and long-term stabilities of proteins, *Adv. Drug Delivery Rev. 46*, 307−326.
22. Ando, S., Putnam, D., Pack, D. W., and Langer, R. (1999) PLGA microspheres containing supercoiled DNA via cryopreparation and carbohydrate stabilization, *J. Pharm. Sci. 88*, 126−130.
23. Studelska, D. R., McDowell, L. M., Adler, M., O'Connor, R. D., Mehta, A. K., Guilford, W. J., Dallas, J. L., Arnaiz, D., Light, D. R., and Schaefer, J. (2003) Conformation of a bound inhibitor of blood coagulant factor Xa, *Biochemistry 42*, 7942−7949.
24. Mehta, A. K., Shayo, Y., Vankayalapati, H., Hurley, L. H., and Schaefer, J. (2004) Structure of a quinobenzoxazine-G-quadruplex complex by REDOR NMR, *Biochemistry 43*, 11953−11958.
25. Gullion, T., and Schaefer, J. (1989) Rotational-echo double-resonance NMR, *J. Magn. Reson. 81*, 196−200.
26. Gullion, T., and Schaefer, J. (1989) Detection of weak heteronuclear dipolar coupling by rotational-echo double-resonance nuclear magnetic resonance, *Adv. Magn. Reson. 13*, 57−83.
27. McDowell, L. M., and Schaefer, J. (1996) High-resolution NMR of biological solids, *Curr. Opin. Struct. Biol. 6*, 624−629.
28. Thompson, L. K. (2002) Solid-state NMR studies of the structure and mechanisms of proteins, *Curr. Opin. Struct. Biol. 12*, 661−669.
29. Günther, H., Ulrich, A. S., and Ramamoorthy, A., Eds. (2004) Special Issue: Solid-state NMR on biological systems, *Magn. Reson. Chem. 42*, 85−300.
30. Yao, J., Nakazawa, Y., and Asakura, T. (2004) Structures of *Bombyx mori* and *Samia cynthia ricini* silk fibroins studied with solid-state NMR, *Biomacromolecules 5*, 680−688.
31. Merritt, M. E., Sigurdsson, S. T., and Drobny, G. P. (1999) Long-range distance measurements to the phosphodiester backbone of solid nucleic acids using ^{31}P-^{19}F REDOR NMR, *J. Am. Chem. Soc. 121*, 6070−6071.
32. Olsen, G. L., Louie, E. A., Drobny, G. P., and Sigurdsson, S. T. (2003) Determination of DNA minor groove width in distamycin−DNA complexes by solid-state NMR, *Nucleic Acids Res. 31*, 5084−5089.
33. Studelska, D. R., Klug, C. A., Beusen, D. D., McDowell, L. M., and Schaefer, J. (1996) Long-range distance measurements of protein binding sites by rotational-echo double-resonance NMR, *J. Am. Chem. Soc. 118*, 5476−5477.
34. Goetz, J. M., and Schaefer, J. (1997) REDOR dephasing by multiple spins in the presence of molecular motion, *J. Magn. Reson. 127*, 147−154.
35. Schaefer, J., and McKay, R. A. (1999) Multi-tuned single coil transmission line probe for nuclear magnetic resonance spectrometer, U.S. Patent 5861748.
36. Gullion, T., Baker, D. B., and Conradi, M. S. (1990) New, compensated Carr-Purcell sequences, *J. Magn. Reson. 89*, 479−484.
37. Gullion, T., and Schaefer, J. (1991) Elimination of resonance offset effects in rotational-echo, double-resonance NMR, *J. Magn. Reson. 92*, 439−442.
38. Stivers, J. T., Pankiewicz, K. W., and Watanabe, K. A. (1999) Kinetic mechanism of damage site recognition and uracil flipping by *Escherichia coli* uracil DNA glycosylase, *Biochemistry 38*, 952−963.
39. Slupphaug, G., Mol, C. D., Kavli, B., Arvai, A. S., Krokan, H. E., and Tainer, J. A. (1996) A nucleotide-flipping mechanism from the structure of human uracil-DNA glycosylase bound to DNA, *Nature 384*, 87−92.
40. Hore, P. J. (1995) *Nuclear Magnetic Resonance*, 1st ed., Vol. 32, Oxford University Press, Oxford, U.K.
41. Gueron, M., and Leroy, J.-L. (1995) Studies of base pair kinetics by NMR measurement of proton exchange, *Methods Enzymol. 261*, 383−413.
42. Jiang, Y. L., Ichikawa, Y., Song, F., and Stivers, J. T. (2003) Powering DNA repair through substrate electrostatic interactions, *Biochemistry 42*, 1922−1929.
43. Dinner, A. R., Blackburn, G. M., and Karplus, M. (2001) Uracil-DNA glycosylase acts by substrate autocatalysis, *Nature 413*, 752−755.
44. Dong, J., Drohat, A. C., Stivers, J. T., Pankiewicz, K. W., and Carey, P. R. (2000) Raman spectroscopy of uracil DNA glycosylase-DNA complexes: insights into DNA damage recognition and catalysis, *Biochemistry 39*, 13241−13250.
45. Drohat, A. C., and Stivers, J. T. (2000) *Escherichia coli* uracil DNA glycosylase: NMR characterization of the short hydrogen bond from His187 to uracil O2, *Biochemistry 39*, 11865−11875.
46. Drohat, A. C., and Stivers, J. T. (2000) NMR evidence for an unusually low N1 pK_a for uracil bound to uracil DNA glycosylase: implications for catalysis, *J. Am. Chem. Soc. 122*, 1840−1841.

BI0483864